Title
DESIGN AND CONSTRUCTION OF THE DONNER 280-CRYSTAL POSITRON RING FOR DYNAMIC TRANSVERSE SECTION EMISSION IMAGING

Author
Derenzo, Stephen E.

Publication Date
1977-09-01

To be presented at the 1977 IEEE
Conference on Decision and Control,
New Orleans, LA, December 7 - 9, 1977

DESIGN AND CONSTRUCTION OF THE DONNER 280-CRYSTAL POSITRON RING FOR DYNAMIC TRANSVERSE SECTION EMISSION IMAGING

Stephen E. Derenzo, Paul G. Banchero, John L. Cahoon,
Ronald H. Huesman, Tony Vuletich, and Thomas F. Budinger

DONNER LABORATORY

September 1977

Prepared for the U. S. Energy Research and
Development Administration under Contract W-7405-ENG-48

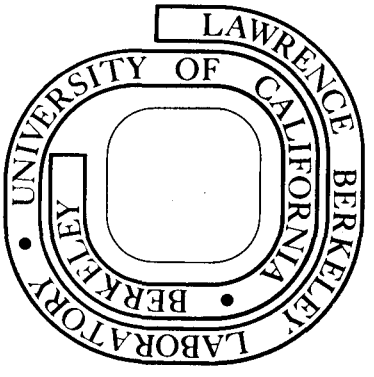

DISCLAIMER

DESIGN AND CONSTRUCTION OF THE DONNER 280-CRYSTAL POSITRON RING FOR DYNAMIC TRANSVERSE SECTION EMISSION IMAGING

Stephen E. Derenzo, Paul G. Banchero, John L. Cahoon,
Ronald H. Huesman, Tony Vuletich, and Thomas F. Budinger

Donner Laboratory
University of California, Berkeley, CA 94720

Abstract

We describe the design and construction of a medical imaging system for the rapid, accurate, three-dimensional imaging of positron-labeled compounds in the human body. Our medical research goals include quantifying blood flow and metabolism in human heart muscle and brain. The system consists of (1) a large gantry containing lead shielding and a ring of 280 NaI(Tl) detectors that completely encircles the patient; (2) 280 photomultiplier tubes, preamplifiers and timing discriminators; (3) circuits that determine whenever a crystal has detected a gamma ray in time coincidence (i.e. within 12 nsec) of any of the opposing 105 crystals and determine the addresses of the crystals involved; (4) 120K words of 12 bit memory for the simultaneous acquisition of data from eight portions of the cardiac cycle; and (5) a hardwired image reconstructor capable of filtering and backprojecting data from 140 views to form a 210 X 210 computed transverse section image in less than 2 sec.

1. Introduction

An important goal of nuclear medicine is the non-invasive quantitative measurement of the concentration of labeled compounds in the human body. The realization of this goal has been made possible through the development of imaging techniques that can depict the three dimensional concentration of activity in the body. The concept underlying these developments is emission computed tomography which is similar in many ways to X-ray computed tomography. The latter, however, looks at the distribution of attenuating material whereas the nuclear medicine techniques can measure the distribution of labeled compounds in various regions of the body and determine how well an organ is functioning. A number of these techniques use collimation to image single-gamma emitters[1-6] while others measure the simultaneous collinear gamma ray pairs produced by positron emitters.[6-18]

The purpose of this paper is to describe a 280 NaI(Tl) crystal positron ring imaging system, now under construction at the Donner Laboratory. This system differs from most other devices in that a large number of small crystals are arranged in a ring that completely encircles the patient (Fig. 1). Lead is used to shield the crystals from activity external to the section being imaged. The device has the potential for dynamic transverse section imaging as the full image of a section is obtained moment by moment without device or patient movement. Our medical research goals include quantifying blood flow and metabolism in human heart muscle and brain.

The use of positrons is motivated by the fact that many short lived positron emitters such as ^{11}C (20 min), ^{15}O (2 min), ^{13}N (10 min), ^{18}F (110 min), and ^{122}I (3.5 min) can be incorporated in molecules of biological importance

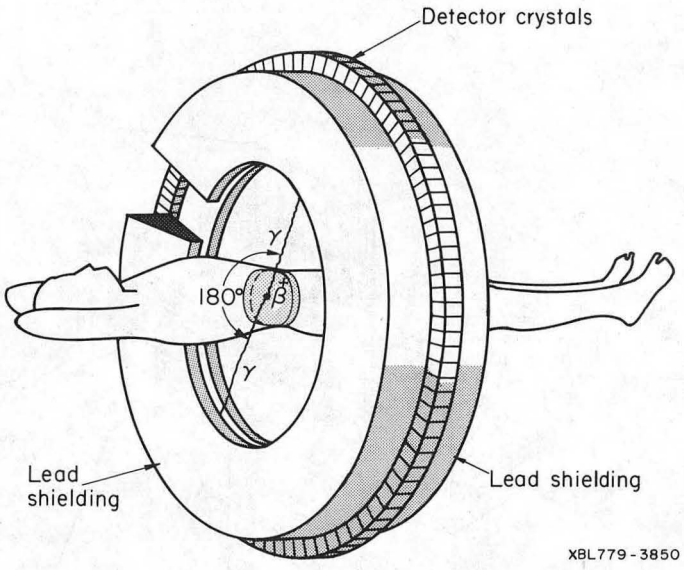

Fig. 1. Arrangement of detector ring and shielding for imaging positron labeled compounds within the body. Whenever a positron is emitted, it annihilates with an electron in the body with the emission of two 511 keV gamma rays in time coincidence and at a relative angle of 180°.

such as amino acids, fatty acids, and sugars. Also, cations such as ^{38}K (8 min) and ^{82}Rb (1.3 min) have a natural affinity for heart muscle and ^{62}Zn has high uptake in the prostate and pancreas.

The isotopes ^{11}C, ^{15}O, ^{13}N, ^{18}F, ^{38}K, ^{52}Fe and ^{62}Zn are available from low energy cyclotrons and ^{82}Rb, ^{68}Ga, and ^{122}I are available from table top generators containing the parent isotopes ^{82}Sr (25 day), ^{68}Ge (275 day), and ^{122}Xe (20 hr), respectively. Between one and 20 millicuries of these short lived isotopes are administered and the dose to the patient is usually less than 1 Rad (whole body) and considerably less for ^{15}O (2 min) and ^{82}Rb (1.3 min). (1 millicurie is 3.7×10^7 radionuclide disintegrations per second and most of the disintegrations result in the emission of a positron.)

2. Description of System

Figure 2 shows a schematic of the gantry that holds the 280 crystals, phototubes, timing discriminators, and lead shielding. The gantry can tilt up to 90° to take angled sections and to image patients in a sitting position. The patient port has a diameter of 50 cm and can accommodate any body part. The thickness of the section being imaged can be varied from 0 to 15 mm by adjusting the position of two lead shields. These shields resemble large tapered lead washers that extend from the 50 cm patient port outward to the 90 cm crystal ring. Each of the 280 crystals is in time coincidence with 105 opposing crystals, resulting in 14,700 crystal pair combinations. These data are arranged into 105 parallel rays (5 mm spatial sampling) for 140 angles (1.3° angular sampling).

2.1 Detector Crystals and Lightpipes

The annihilation gamma ray detector consists of a ring of closely packed 8 mm × 30 mm × 50 mm deep NaI(Tl) crystals. In order to couple these crystals to readily available 38 mm bialkali phototubes, we designed a special set of quartz lightpipes directing the scintillation light from each crystal into one of five directions (-90°, -60°, 0°, 60°, 90°) to provide sufficient separation for mounting the phototubes (Fig. 3). This awkward design could be avoided if high quality rectangular phototubes were available. Rectangular NaI(Tl) crystals were chosen over the more commonly used cylindrical crystals to maximize the detection solid angle. The 8 mm dimension was chosen to provide sufficient resolution to distinguish epi- from endocardium; the 30 mm dimension was chosen to permit sections as thick as 15 mm to be imaged; and the 50 mm depth was chosen to provide detection efficiency without excessive scattering and multiple detections in the crystals.

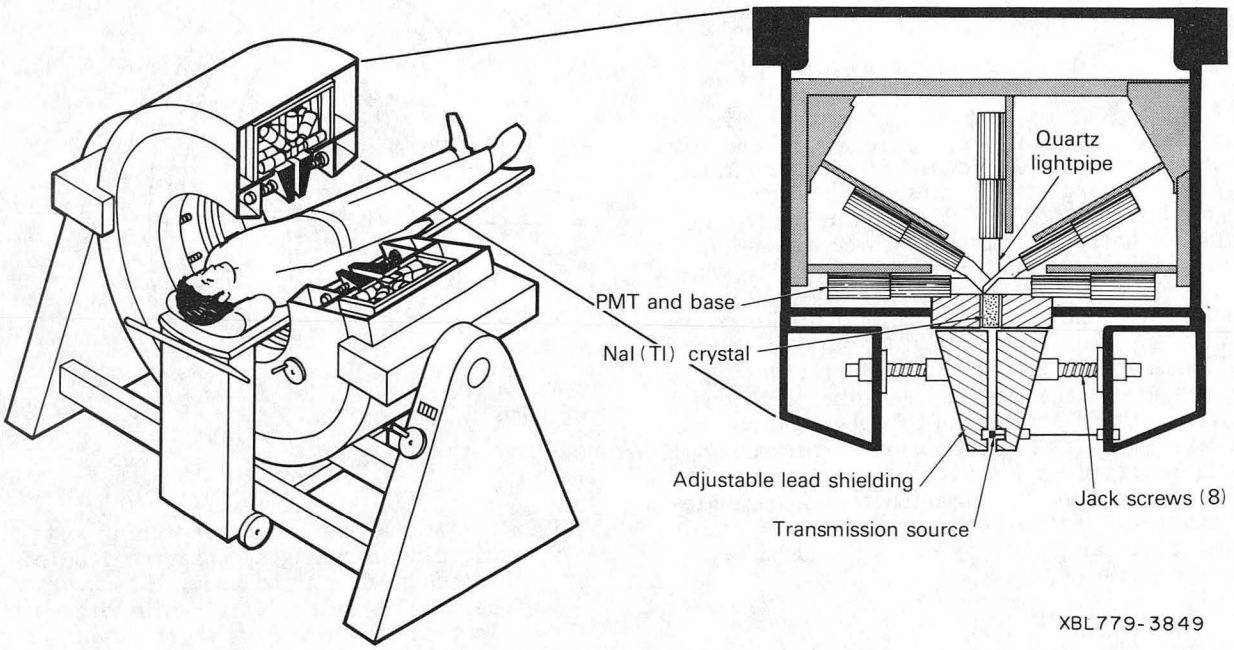

Fig. 2. Schematic of Donner 280 crystal positron ring camera. Crystals are mounted behind adjustable lead shielding and are individually coupled to phototubes via quartz lightpipes.

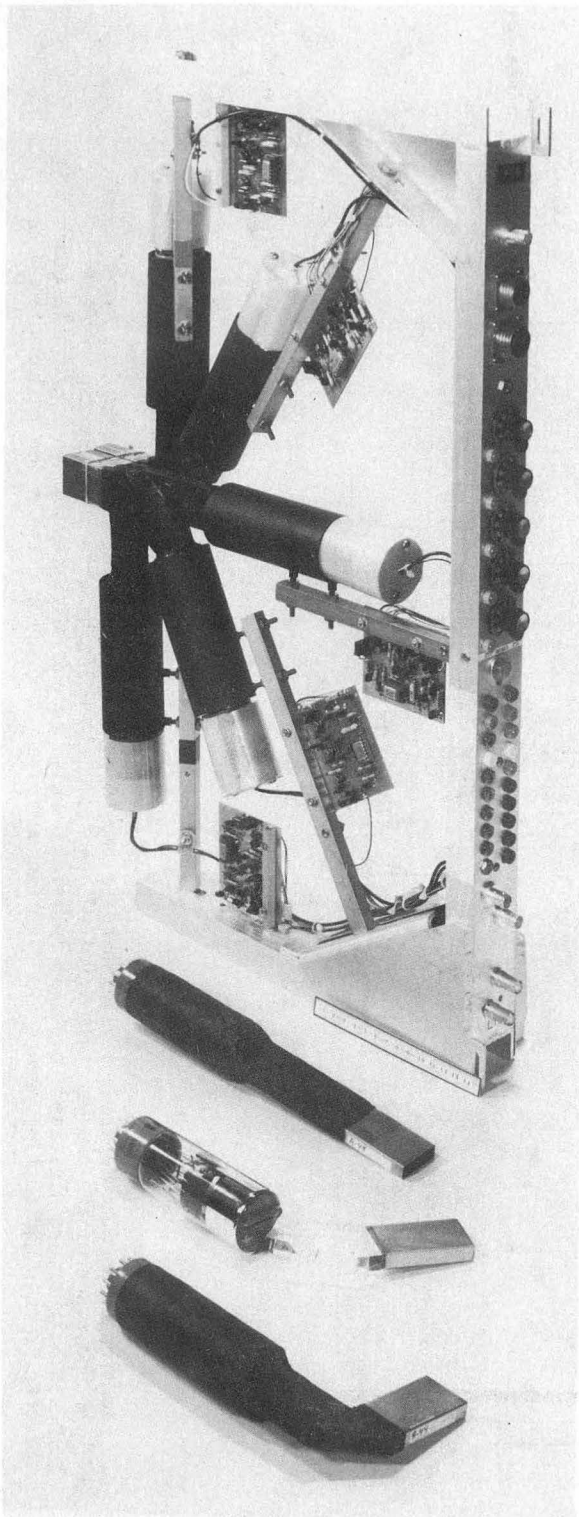

Fig. 3. Set of five crystals, lightpipes, phototubes, bases and timing discriminators mounted in an aluminum frame. Fifty-six of these frames will be mounted in the gantry shown in Fig. 2. Individual detector assemblies (0°, 60°, and 90°) are shown in the lower portion of the picture. The 60° assembly is shown without aluminum foil and black tape.

When these crystals are coupled directly to a bialkali phototube, the 511 keV photopeak resolution ranges from 8 to 10% FWHM. Using the 0°, 60°, and 90° quartz lightpipes shown in Fig. 3 the light loss is 30%, 40%, and 45%, respectively and the 511 keV photopeak resolutions range from 10% to 15% FWHM. At 511 keV the individual crystals have a photopeak detection efficiency of 25% and for pulses above 100 keV the detection efficiency is 60%. For a closely packed group of crystals this efficiency is reduced to 45% through the rejection of detections involving 2 or more neighboring crystals.

2.2 Ring Electronics

As shown in Fig. 3 each group of five crystals, lightpipes and phototubes is mounted in a "U" shaped aluminum frame. In close proximity to each phototube base is a small printed circuit card containing a pulse height adjustment, a preamplifier, two timing discriminators, and an emitter follower (Fig. 4). The output of the preamplifier is adjusted to deliver a -5V photopeak pulse to the timing discriminators and emitter follower. The lower (2 keV) discriminator establishes an accurate timing pulse and the higher (50 keV) discriminator is used by the circuit to reject low energy X-rays and small phototube noise pulses. The timing differences among the 280 phototube channels are compensated by adjusting RC integrators located on the frames between the 2 keV discriminators and the 100 nsec one-shots. Analog pulses from the emitter followers are summed on the frames in groups of eight. The 560 digital signals (2 keV and 50 keV discriminators for 280 channels) and the 35 analog signals (sums for 35 groups of 8) are sent by cables from the gantry to the coincidence and address logic cards located in a separate electronics rack. The circuits shown in Fig. 4 identify whenever any of the 35 groups is in time coincidence with its opposing 14 groups. Two coincidence gates are used on each card, one for "on time" events and another for "off time" events. The coincidence delay progressively increases from card to card so that the delay differences between opposing groups of eight always exceed 50 nsec. Since the "on time" events include true coincidences as well as unwanted accidental coincidences, it is helpful to record simultaneously a statistically equivalent sample of pure accidental events for subsequent background subtraction.

The resolving time of the detectors and timing discriminators is 5 nsec FWHM and 10 nsec FW(0.1)M. A 12 nsec timing window includes almost all the true coincidences and provides a small allowance for drifts in timing. When the coincidence gates on two cards are activated, the addresses of the involved crystals are determined and the analog pulse height information is gated to a pair of analog to digital converters. The deadtime for this process is 400 nsec. The event is rejected whenever more than two groups of eight are involved or whenever more than one crystal in each group of 8 has detected a gamma

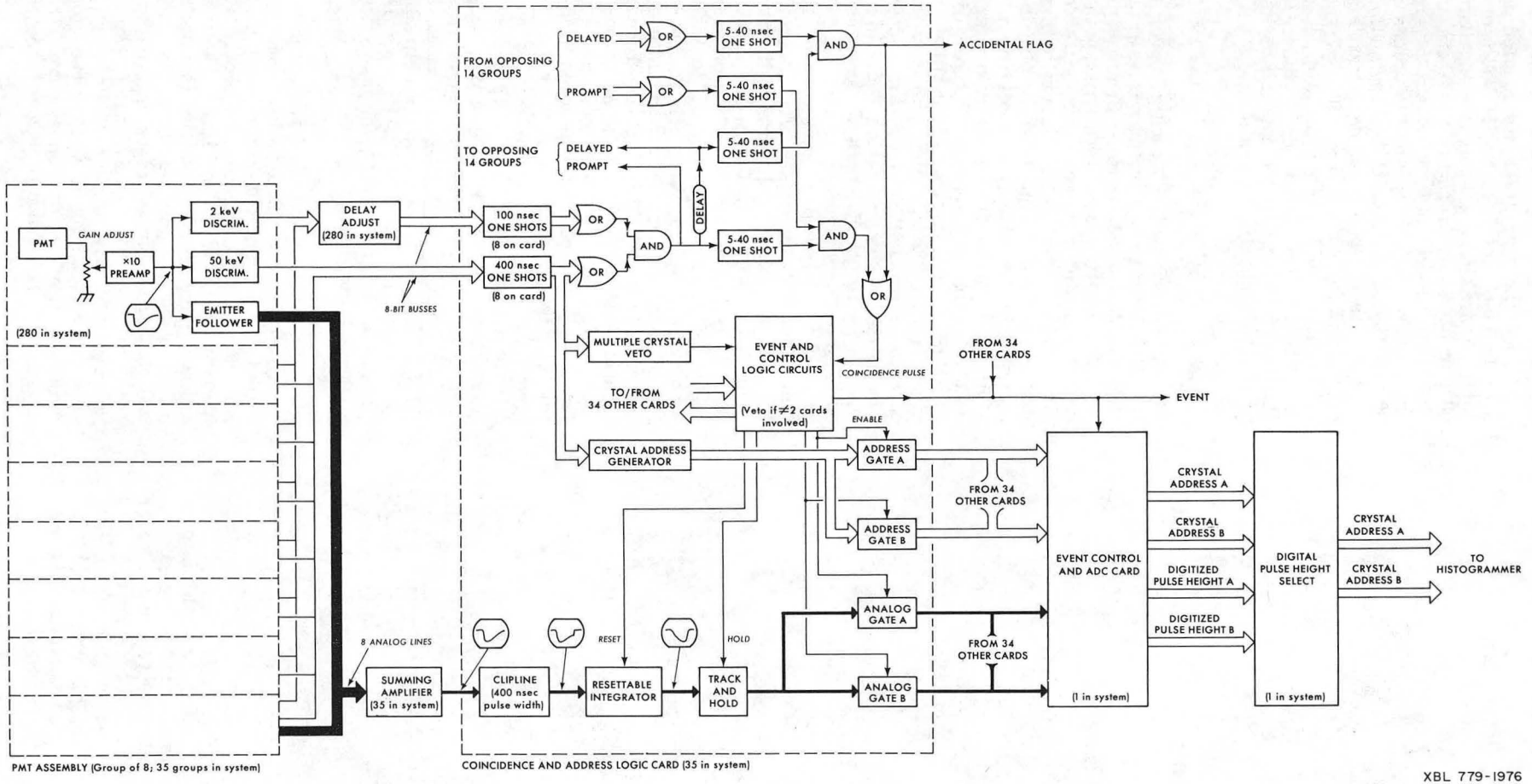

Fig. 4. Electronics used to determine: (1) whenever two opposing crystals detect a coincident event; (2) the addresses of the two crystals involved; and (3) the pulse heights in those two crystals. The pulse heights are digitized to permit individual pulse height selection for each crystal. Both accidental events and on-time events are simultaneously recorded. For details see text section 2.2.

within the last 400 nsec. A clipline in the analog circuit cancels the scintillation decay tail electronically so that gamma rays detected more than 400 nsec apart do not interfere. The pulse heights are digitized to permit individual pulse height selection for each phototube. This is necessary when using photopeak selection because the day to day phototube gain shifts typically exceed 10%.

2.3 Data Histogramming and Storage

After pulse height selection, crystal pair addresses are converted into parallel ray coordinates (angle and position) by a hard-wired logic circuit (Fig. 5). Each of the 14,700 rays that pass through the 50 cm patient port corresponds to a 12-bit word on a 15K CMOS memory board. For each "on time" event, the appropriate word is read out from memory, incremented by one, and read back. For real-time accidental background subtraction, "off time" events cause the word in memory to be decremented. In this way events are accumulated or "histogrammed". The dead time is about 1 μsec.

The histogrammer contains eight memory boards in order to handle gated cardiac studies. Data collection starts on the R-wave of an EKG signal and for some preset time interval, usually 100 msec, all events are histogrammed in memory board 1; for the second time interval all events are histogrammed in memory board 2. The process continues until all eight memory boards have been sequenced or until a new R-wave re-initiates the procedure. To accumulate sufficient statistics, data are collected over many cardiac cycles for 5 to 10 minutes.

At the conclusion of the study, data from each of the memory boards are transferred to remote storage on a DEC RK-05 disc system with removable disc cartridges. The disc file is handled by a DEC PDP-11/10 CPU and data for 80 images can be accumulated on a single disc cartridge. The histogrammer allows data acquisition on one board while simultaneously transferring data to disc from another board. This feature permits up to eighty sequential images as short as 0.5 sec to be taken for blood flow studies.

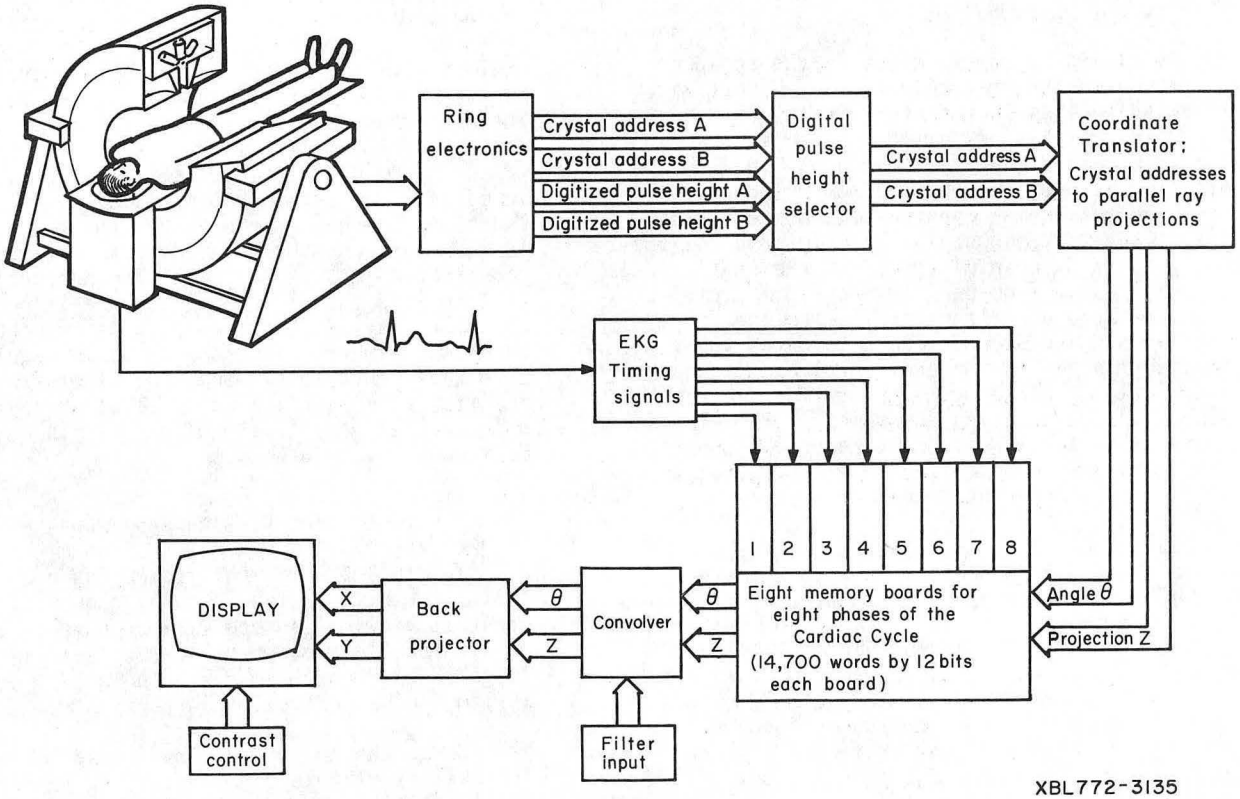

Fig. 5. Overall system configured for gated cardiac imaging. Data from the ring electronics are sent successively to eight different memory boards for each of eight portions of the cardiac cycle. The eight reconstructed images can be displayed in sequence to depict a motion image of the heart averaged over several minutes.

2.4 Accidental and Scatter Background Subtraction

After the positron is emitted by the labeled compound, it travels a few mm in the tissue (the distance depending on its energy)[19,20] and annihilates with a nearby electron. The 511 keV photons fly off toward the detectors, but most are scattered enroute. Three classes of coincident events are detected:

(1) True events: both detected photons originated from the same positron and neither have scattered in tissue.

(2) Scattered events: both detected photons originated from the same positron but one or both have scattered in tissue.

(3) Accidental events: the two photons originated from different positrons and were detected within the coincidence resolving time by chance. Note that this background can be reduced by improving the coincidence resolving time or by reducing the amount of activity.

Only true events provide useful image information, while the scattered and accidental events produce a broad, heterogeneous background on the true image. Most positron imaging systems can image patients at 10,000 events per second but typically 10 to 20% of these are accidental events and 10 to 20% are scattered events. For quantitative work it is necessary to subtract both of these backgrounds.

To permit the subtraction of the accidental background, events are collected in an "off time" window as well as in the usual "on time" window. There are two ways of performing the subtraction. The first method involves recording "on time" and "off time" events in separate memory boards. Since the accidental events (represented by the "off time" events) contain only low spatial frequencies, it is helpful to reduce the statistical fluctuations by smoothing the "off time" projection data before subtracting it from the "on time" data. The second method involves the real time subtraction of the accidental background by incrementing the histogram memory for "on time" events and decrementing the memory for "off time" events. The latter method is necessary when eight images must be collected almost simultaneously, such as for gated cardiac studies.

Unfortunately, the scattered background events are in true time coincidence and are not removed by subtracting the "off time" events. We propose to approximate the shape of the scatter background image by smoothing the emission image with an empirical function. Then this "background image" is subtracted from the emission image with the amplitude that gives the best cancellation in areas where there is no activity (such as below the patient bed). A more rigorous approach would calculate the shape of the scatter background from the known distributions of emission and attenuation, but the numerical integrations may be too time consuming for routine evaluation.

2.5 Attenuation Corrections

The effect of attenuation by scattering in the body is severe and in only about 20% of the annihilations do both gamma rays escape the body unscattered. Fortunately the attenuation corrections are readily measured by using an external positron source prior to the administration of positron labeled compounds. Since the attenuation for collinear 511 keV annihilation gamma ray pairs depends only on their line of flight and not on the position of the point of annihilation, the attenuation correction factor for each of the 14,700 coincident detector pairs is the ratio of the transmitted flux before and after the patient is positioned in the system. In the PETT III system, a hoop source of positron emitter was manually inserted at the periphery of the patient port.[13] In our system, a hoop containing the positron emitter ^{68}Ge (half-life 275 days) can be moved by remote control from a groove in the lead shielding to the center of the shielding gap (Fig. 2). The data are used both to correct the emission image and are reconstructed to provide a transmission image containing useful anatomical landmarks.

2.6 Reconstruction and Display

After accidental background subtraction and correction for attenuation, reconstruction is performed by a hardwired convolver and backprojector utilizing the widely used convolution algorithm. For work in this area, see Ref. 21. The projection data called in from disc storage consist of 105 parallel rays at 140 angles between 0° and 180° and are stored as 12-bit scaled integers. The data are convolved with a filter function chosen by the user and the filtered projections are then backprojected to form the reconstructed image. The total reconstruction time will be less than 2 seconds and the image is a 210 X 210 array of 24-bit words. After scatter background subtraction, the image is a quantitative representation of the isotope distribution in the transverse section and will be displayed on a commercial grey level CRT or used in compartment model calculations.

3. Test Results and Images

The full 280 crystal system has been physically simulated by two opposing groups of eight crystals viewing isotope-filled phantoms rotated on a turntable between them. See Ref. 17 for details and phantom images. In Table 1 we summarize the properties of our system.

Using the 16 crystal imaging setup, we tested the ability of this mode of imaging to detect ischemia and infarction in the human myocardium. A human chest phantom 20 cm by 28 cm was built in three parts to simulate the chest wall, lungs, and heart. The heart contained 9 separate compartments to simulate portions of the myocardium

TABLE 1. Properties of the Donner 280 Crystal Positron Ring System

Number of NaI(Tl) Crystals	280
Crystal Size	8 mm × 30 mm × 50 mm deep
Diameter of Crystal Ring	90 cm
Diameter of Patient Port	50 cm
Number of Opposing Crystals in Coincidence with Each Crystal	105
Number of Projection Rays Measured	14,700 (140 angles X 105 rays)
Image Resolution	7.5 mm FWHM at ring center[a]
Event Rates for 200 μCi per 1 cm section of a 20 cm diam cylinder of water:[b]	
True Coincidence Rate	6,000 per sec[c]
Accidental Coincidence Rate	1,400 per sec
Scattered Coincidence Rate	1,200 per sec

[a] 10 cm from the ring center the point spread function is elliptical with 8 mm × 12.5 mm FWHM.

[b] Based on measurements made using two opposing groups of eight crystals and a 10 mm section thickness. Backgrounds estimated for a 30cm diam region of interest. For details, see Ref. 17.

[c] Corresponds to a sensitivity of 10,000 true events/sec per $\mu Ci/cm^3$ in a 20 cm diam cylinder of water. This sensitivity is doubled by increasing the section thickness from 10 mm to 15 mm.

(Fig. 6). The compartments were filled with various concentrations of ^{62}Zn chloride to simulate viable or ischemic myocardium. ^{62}Zn was chosen because its maximum positron energy is close to that of ^{82}Rb (∿3 MeV). The results show that 100,000 events are sufficient to reliably image 1.5 cm regions of transmural infarction. With 350,000 detected events, endocardial ischemia of 50% was visualized as an enlargement of the left ventricle.

4. Expected Medical Applications

We expect that this system will allow us to image the myocardial uptake of ^{82}Rb (half-life 1.3 min.) and the metabolism of amino acids labeled with ^{11}C (half-life 20 min.) with a resolution of 10 mm FWHM and a statistical uncertainty of 20%. To image the beating heart with 10 mm resolution we will send data to 8 different memories based on the timing from an EKG signal. For imaging relatively static organs, such as the brain, liver, kidneys or pancreas, gated imaging is not necessary and adequate data can be collected in a few minutes to give a resolution of 8 mm FWHM and 5% uncertainty.

One of the great medical advantages of this instrument is its ability to measure brain blood flow. Due to the limitations in statistics, however (10,000 events per one sec frame) we cannot expect to achieve a resolution better than 20 mm FWHM with 20% uncertainty.[6]

5. Future Improvements

An improvement in resolution to about 6 mm FWHM and an increase in sensitivity by a factor of 15 is possible using three rings of bismuth germanate detector crystals[22,23] and rectangular phototubes. This would permit the simultaneous visualization of 5 sections (using cross coincidences) and permit improved dynamic function studies of whole organs. Though the expense is great the unique medical science research potentials outweigh the costs.

ACKNOWLEDGMENTS

We are indebted to G. Gates for mechanical design of the gantry; to W. Greenberg for aid in data analysis and image reconstruction; and to Y. Yano and G. Roth for providing ^{68}Ga and ^{62}Zn isotopes. This work was supported by NCI grant No. R01 CA-17566-01, NCI contract No. NIH Y01-CB-50304 and by the Energy Research and Development Administration.

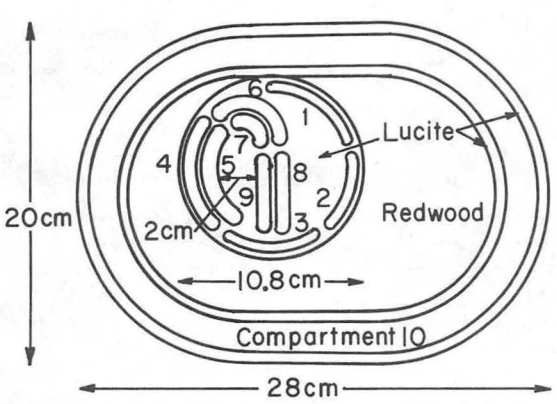

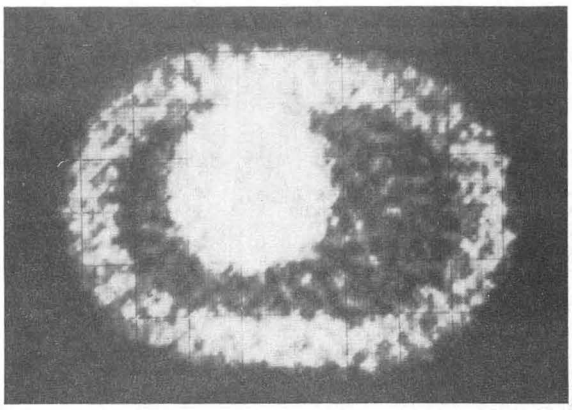

Transmission

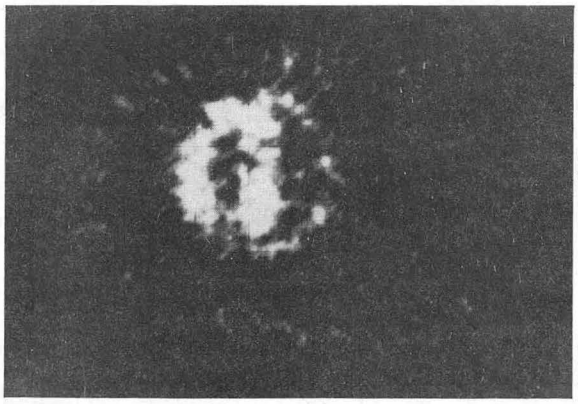

100,000 events
all compartments full

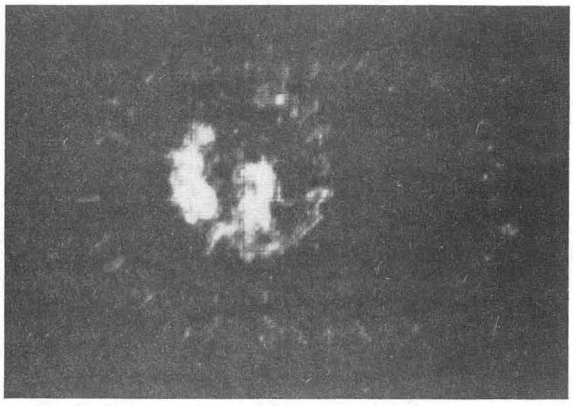

100,000 events
compartments 6 & 7 cold

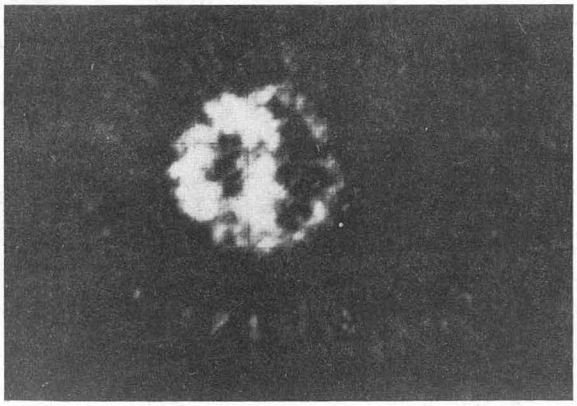

350,000 events
all compartments full

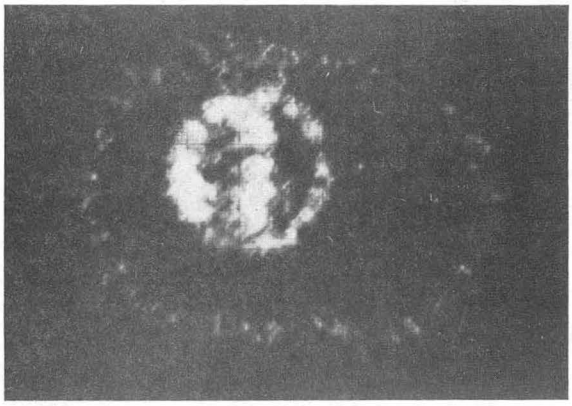

350,000 events
concentration in compartments
5, 7, 9 reduced to 50%

Fig. 6. Images of a human thorax phantom. Top row gives dimensions of heart muscle compartments, lungs, and chest wall and shows a transmission image using an external ^{68}Ga source. Center row shows that 100,000 ^{62}Zn emission events are sufficient to detect an anterior transmural infarction. Bottom row shows that with 350,000 events a 50% endocardial ischemia is visualized as an enlargement of the left ventricle.

REFERENCES

1. Kuhl, D. E. and R. Q. Edwards, "Image Separation Radioisotope Scanning", Radiology 80, 653-662, 1963.

2. Kuhl, D. E., E. J. Hoffman, M. E. Phelps, et al., "Design and Application of the Mark IV Scanning System for Radionuclide Computed Tomography of the Brain", IAEA Symposium on Medical Radionuclide Imaging, Los Angeles, California, 1976. (In press).

3. Budinger, T. F. and G. T. Gullberg, "Transverse Section Reconstruction of Gamma-ray Emitting Radionuclides in Patients", in Reconstruction Tomography in Diagnostic Radiology and Nuclear Medicine, M. M. Ter-Pogossian et al., Eds., University Park Press, Baltimore 1977, pp. 315-342.

4. Jaszczak, R. J., P. H. Murphy, D. Huard, and J. A. Burdine, "Radionuclide Emission Computed Tomography of the Head with ^{99m}Tc and a Scintillation Camera", J. Nucl. Med. 18, 373-380, 1977.

5. Keyes, J. W. Jr., N. Orlandea, W. J. Heetderks, P. F. Leonard, and W. L. Rogers, "The Humongotron - A Scintillation-Camera Transaxial Tomograph", J. Nucl. Med. 18, 381-387, 1977.

6. Budinger, T. F., S. E. Derenzo, G. T. Gullberg, W. L. Greenberg, and R. H. Huesman, "Emission Computer Assisted Tomography with Single-Photon and Positron Annihilation Photon Emitters", J. Comput. Assisted Tomography 1, 131-145, 1977.

7. Rankowitz, S., J. S. Robertson, W. A. Higinbotham, et al., "Positron Scanner for Locating Brain Tumors", IRE Int. Conv. Record 10(9), 49-56, 1962.

8. Robertson, J. S., R. B. Marr, M. Rosenblum, et al., "32 Crystal Positron Transverse Section Detector", in Tomographic Imaging in Nuclear Medicine, pp. 142-153, G. S. Freedman, Ed., Society of Nuclear Medicine, New York, 1973.

9. Brownell, G. L., C. A. Burnham, D. A. Chesler, et al., "Transverse Section Imaging of Radionuclide Distributions in Heart, Lung and Brain", in Reconstruction Tomography in Diagnostic Radiology and Nuclear Medicine, M. M. Ter-Pogossian et al., Eds., University Park Press, Baltimore 1977, pp. 293-308.

10. Correia, J. A., D. A. Chesler, B. Hoop, Jr., et al., "Transverse Section Reconstruction with Positron Emitters and the MGH Positron Camera", J. Nucl. Med. 17, 551, 1976.

11. Lim, C. B., D. Chu, L. Kaufman, et al., "Initial Characterization of a Multiwire Proportional Chamber Positron Camera", IEEE Trans. Nucl. Sci. NS22(1), 388-394, 1975.

12. Muehllehner, G., M. P. Buchin, and J. H. Dudek, "Performance Parameters of a Positron Imaging Camera", IEEE Trans. Nucl. Sci. NS23(1), 528-537, 1976.

13. Phelps, M. E., E. J. Hoffman, N. A. Mullani, et al., "Application of Annihilation Coincidence Detection to Transaxial Reconstruction Tomography", J. Nucl. Med. 16, 210-224, 1975.

14. Hoffman, E. J., M. E. Phelps, N. A. Mullani, C. S. Higgins, and M. M. Ter-Pogossian, "Design and Performance Characteristics of a Whole-Body Positron Transaxial Tomograph ", J. Nucl. Med. 17, 493-502, 1976.

15. Cho, Z. H., M. B. Cohen, M. Singh, et al., "Performance and Evaluation of the Circular Ring Transverse Axial Positron Camera (CRTAPC)", IEEE Trans. Nucl. Sci. NS24(1), 532-543, 1977.

16. Derenzo, S. E., H. Zaklad, and T. F. Budinger, "Analytical Study of a High-Resolution Positron Ring Detector System for Transaxial Reconstruction Tomography", J. Nucl. Med. 16, 1166-1173, 1975.

17. Derenzo, S. E., T. F. Budinger, J. L. Cahoon, R. H. Huesman, and H. G. Jackson, "High Resolution Computed Tomography of Positron Emitters", IEEE Trans. Nucl. Sci. NS24(1), 544-558, 1977.

18. Yamamoto, Y. L., C. J. Thompson, E. Meyer, et al., "Dynamic Positron Emission Tomography for Study of Cerebral Hemodynamics in a Cross Section of the Head Using Positron-Emitting ^{68}Ga-EDTA and ^{77}Kr", J. Comput. Assisted Tomography 1, 43-56, 1977.

19. Phelps, M. E., E. J. Hoffman, S. C. Huang, et al., "Effect of Positron Range on Spatial Resolution", J. Nucl. Med. 16, 649-652, 1975.

20. Cho, Z. H., J. K. Chan, L. Eriksson, et al., "Positron Ranges Obtained from Biomedically Important Positron-Emitting Radionuclides", J. Nucl. Med. 16, 1174-1176, 1975.

21. Special issue on Physical and Mathematical Aspects of 3-D Image Reconstruction, IEEE Trans. Nucl. Sci. NS21(3), 1974.

22. Cho, Z. H. and M. R. Farukhi, "Bismuth Germanate as a Potential Scintillation Detector in Positron Cameras", J. Nucl. Med. 18, 840-844, 1977.

23. Derenzo, S. E., "Positron Ring Cameras for Emission-Computed Tomography", IEEE Trans. Nucl. Sci. NS24(2), 881-885, 1977.

TECHNICAL INFORMATION DEPARTMENT
LAWRENCE BERKELEY LABORATORY
UNIVERSITY OF CALIFORNIA
BERKELEY, CALIFORNIA 94720